



CHORUS

This is the accepted manuscript made available via CHORUS. The article has been published as:

Ballooning in spiders using multiple silk threads

Charbel Habchi and Mohammad K. Jawed

Phys. Rev. E **105**, 034401 — Published 4 March 2022

DOI: [10.1103/PhysRevE.105.034401](https://doi.org/10.1103/PhysRevE.105.034401)

Ballooning in Spiders using Multiple Silk Threads

Charbel Habchi*

Notre Dame University-Louaize, Mechanical Engineering Department, 1200 Zouk Mosbeh, Lebanon.

Mohammad K. Jawed†

*University of California, Los Angeles, Department of Mechanical
and Aerospace Engineering, Los Angeles, California 90095, USA.*

(Dated: February 7, 2022)

In this paper, three-dimensional numerical simulations of ballooning in spiders using multiple silk threads are performed using the discrete elastic rods method. The ballooning of spiders is hypothesized to be caused by the presence of the negative electric charge of the spider silk threads and the positive electric potential field in the earth's atmosphere. The numerical model presented here is first validated against experimental data from the open literature. After which, two cases are examined, in the first it is assumed that the electric charge is uniformly distributed along the threads while in the second, the electric charge is located at the thread tip. It is shown that the normalized terminal ballooning velocity, i.e. the velocity at which the spiders balloon after they reach steady-state, decrease linearly with the normalized lift force, especially for the tip located charge case. For the uniform electric charge case, this velocity shows a slightly weaker dependence on the normalized lift force. Moreover, it is shown in both cases that the normalized terminal ballooning velocity has no dependence on the normalized elastic bending stiffness of the threads and on the normalized viscous forces. Finally, the multi-thread bending process shows a three-dimensional conical sheet. Here we show that this behavior is caused by the Coulomb repelling forces owing to the threads electric charge which leads to dispersing the threads apart and thus avoid entanglement.

I. INTRODUCTION

Ballooning is the mechanism of dispersal of wingless arachnids, mainly spiders, to which a silk thread is attached [1]. Even though, spiders do not have wings to fly, two centuries ago, Charles Darwin observed hundreds of ballooning spiders landing on the HMS Beagle located 60 miles offshore [2]. This peculiar observation, at that time, was also reported earlier in the 17th and 19th centuries [3, 4] and it was commonly occurring on relatively calm days with low wind speed, below 3 m/s [5–9].

Since these observations [3, 4], two competing theories were associated to explain the ballooning of spiders. In the first, ballooning of spiders is associated to natural convection currents caused by the thermal gradients in the earth boundary layer. It is assumed that these rising currents create drag forces on the light spider threads which induce lift forces when they overcome the weight of the spider. This hypothesis was extensively studied by several authors [7, 10–13]. For instance, Zhao *et al.* [14] used a fully coupled fluid-structure interaction two-dimensional numerical model with the immersed boundary method (IBM) to analyze the effect of spider mass and thread length on the ballooning dynamics. They also analyzed the effect of vortex shedding, mainly at the trailing edge of the thread, on the oscillations and deformation of the spider silk threads during ballooning. This study is based on several assumptions neglecting the thread mass and thickness as well as representing the spider by a point mass. Suter [15] studied the condition of airflow on spider ballooning, and highlighted the possibility that atmospheric turbulence may affect the ballooning and dispersal of spiders. Other authors studied the effect of atmospheric turbulence on the ballooning of spiders and on the bending of the silk threads [16, 17]. For instance, Reynolds *et al.* [16] modeled the dynamics of fully elastic silk thread in isotropic and homogeneous turbulent flows. The thread is modelled by a chain of spheres attached by springs. In their study they highlight the fact that the threads are highly twisted and bent due to turbulent structures which impede the aerodynamic control of ballooning. This fact was not captured earlier by Humphrey [10] who modeled the spider thread by rigid inextensible massless cylindrical rod aligned with the wind direction. Meanwhile, the effect of the electric charge of spider silk threads [18] on the thread unfolding dynamics is not included in these aforementioned studies [13]. This electric charge may induce Coulomb repelling forces which can have an important role in keeping the threads apart to avoid entanglement which may explain the three-dimensional conical sheet shape of the silk threads.

* charbel.habchi@ndu.edu.lb

† khalidjm@seas.ucla.edu

34 In the second hypothesis, ballooning of spiders is associated to the electrostatic force caused by the interaction
 35 between the Earth's electric field and the electric charge of spider silk threads. This electrostatic buoyancy creates
 36 a lift force on the threads which may cause spiders ballooning under certain conditions [19–21]. While, the first
 37 hypothesis discussed in the previous section is extensively analyzed in the open literature, the effect of electrostatic
 38 force on ballooning of spiders is still not fully studied and it was first introduced recently by Gorham [19]. Gorham
 39 [19] developed a simplified theoretical model of a spider with a single thread showing that the electrostatic force
 40 caused by the atmospheric potential gradient and the charged threads could be responsible for spiders take-off and
 41 ballooning. For instance, it is found [19] that a single silk thread electric charge of 100 nC is needed to lift a spider
 42 weighting 1 mg under standard atmospheric electric potential over flat field of 120 V/m [19]. From experimental
 43 observation Morley and Robert [21] showed that spider mechanosensory hairs can detect electric fields which in its
 44 turn triggers the ballooning behavior. This could explain why spiders prefer to balloon from prominence, such as
 45 trees, where the electric field is higher than that on flat fields [21]. Recently, Morley and Gorham [22] conducted
 46 experimental measurements on ballooning behavior inside a closed chamber in which they control the electric field
 47 with no significant air motion. Coupling their experimental data to a physical one-dimensional model, they estimated
 48 that the total thread charge required for ballooning is around 1.15 nC for spiders weighting 0.9 mg, i.e. 1.28 nC/mg.
 49 In their experiment, they consider *Erigone* spiders on the tip of a conductive launch point subjected to an electric
 50 field strength of about 1 kV/m, similar to those observed around the tips of tree branches.

51 Meanwhile, in all these studies, there is no investigation on multi-thread spider ballooning process neither on the
 52 effect of the electrostatic repelling force on the terminal shape of the threads and the ballooning velocity [13]. Thus,
 53 in the current paper we develop a new three-dimensional numerical model including the viscous forces, weight and
 54 dimensions of the thread and spider, electrostatic lift force and repelling forces and the elastic bending force to explore
 55 the ballooning and unfolding dynamics of spider silk threads. This can help for instance in designing new types of
 56 ballooning sensors to explore the atmospheric properties [23].

57 This paper is organized as follows, in section II A we state the problem and the physical parameters such as the
 58 spider weight, electric field, silk thread charge, viscous forces, and silk thread properties. In section II B we present
 59 the numerical method and governing equations for the ballooning spider. Section III is devoted to the results and
 60 discussions and in section IV we present the concluding remarks.

61 II. METHODOLOGY

62 A. Problem Definition

63 It is still unclear on how spiders can emit silk threads loaded with static electric charge. According to the literature,
 64 this could be done during the spinning process where the threads are rapidly loaded with the electric charge, or this
 65 could happen after the spinning process due to friction with the air flow [18, 19].

66 In the present study, the spider is approximated by a sphere attached to n_t silk threads initially extended vertically
 67 and very close to each other with a distance of 100 μm . A schematic of the spider with its threads during typical
 68 ballooning is shown in Figure 1.

69 The size and mass of the spider are chosen based on *Erigone* spiders studied by Morley and Gorham [21, 22] where
 70 the spider mass is considered $m_s = 1$ mg and its size is $r_s = 1$ mm. The typical electric charge of the spider body Q_s
 71 is assumed 3 pC [22]. The acceleration of gravity is $g = 9.81$ m/s² pointing downward. The spider silk thread density
 72 is taken $\rho_t = 1200$ kg/m³ [24] with a radius $r_t = 300$ nm [17, 22].

73 The forces acting on the spider and threads are listed in this section. The weight of the spider and threads are
 74 given respectively by:

$$W_s = m_s g \quad (1)$$

$$W_t = n_t \rho_t \pi r_t^2 l_t \quad (2)$$

75 where l_t is the length of one thread, m_s the spider mass, n_t the number of threads, ρ_t the thread density and r_t the
 76 thread radius.

77 The characteristic elastic bending force of the threads is expressed as:

$$E_b = \frac{YI}{l_t^2} \quad (3)$$

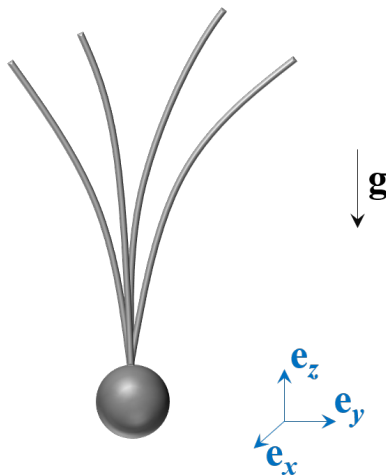


FIG. 1: Schematic of the spider represented by a sphere of radius r_s and several threads of length l_t and radius r_t

78 where Y is the thread's Young modulus and $I = \frac{\pi r_t^4}{4}$ is the area moment of inertia of the silk thread.

79 The Coulomb repulsion force acting on the threads is given by the Coulomb's inverse-square law:

$$F_r = k_e \frac{|q_1 q_2|}{r^2} \quad (4)$$

80 where $k_e = 9 \times 10^9 \text{ Nm}^2\text{C}^{-2}$ is the Coulomb constant, q_1 and q_2 are the signed magnitudes of the charges of the spider
81 threads, and r is the distance between the threads.

82 The electrostatic force of the threads and the spider is given by the following expression:

$$F_l = E(Q_t + Q_s) \quad (5)$$

83 where E is the earth electric field, Q_t and Q_s are the total charges of the silk threads and spider, respectively.

84 Finally the hydrodynamic forces F_v on the spider and threads are computed using the Resistive Force Theory
85 (RFT) as explained in the next section.

86 In this paper we run parametric sweep simulations by varying the forces acting on the spider and analyzing the
87 normalized terminal ballooning velocity, which is the normalized speed at which the spider is ballooning when it
88 reaches steady-state. Moreover, the unfolding dynamics of the spider threads under the coupled effect of electrostatic
89 and viscous forces are studied.

90 B. Numerical Method for Ballooning Spiders

91 The numerical method adopted to study the fluid-structure-electric field interaction combines three components.
92 The first component concerns the Discrete Elastic Rod (DER) method to compute the elastic deformation of the
93 threads [25], i.e., bending, twisting, and stretching, with the primary mode of deformation being bending. The
94 second component is the RFT adopted to compute the hydrodynamic viscous forces on the spider and threads [26],
95 and finally the third component is the electrostatic forces caused by the atmospheric potential gradient and the silk
96 electric charge.

97 The numerical simulations in this paper employ a discrete kinematic representation of the spider following the
98 DER algorithm [25, 27, 28]. In Figure 2(a), the spider is modeled as a network of elastic rods with one node, \mathbf{x}_0 ,
99 representing the spider body and N_t nodes per thread. For a spider with n_t threads, the total number of nodes is
100 $n_t N_t + 1$. The vector between two consecutive nodes is an "edge" and each thread is composed of N_t edges. The
101 edges, \mathbf{e} , on the j -th thread are

$$\begin{aligned}
\mathbf{e}^{N_t(j-1)+0} &= \mathbf{x}_{N_t(j-1)+1} - \mathbf{x}_0, \\
\mathbf{e}^{N_t(j-1)+1} &= \mathbf{x}_{N_t(j-1)+2} - \mathbf{x}_{N_t(j-1)+1}, \\
\mathbf{e}^{N_t(j-1)+2} &= \mathbf{x}_{N_t(j-1)+3} - \mathbf{x}_{N_t(j-1)+2}, \\
&\dots, \\
\mathbf{e}^{N_t j-1} &= \mathbf{x}_{N_t j} - \mathbf{x}_{N_t j-1}.
\end{aligned}$$

102 Note that an edge can be usually defined as $\mathbf{e}^i = \mathbf{x}_{i+1} - \mathbf{x}_i$ (i.e. vector connecting two consecutively numbered
103 nodes), except the first edge on each thread. The total number of edges for a spider with n_t threads is $n_t N_t$.

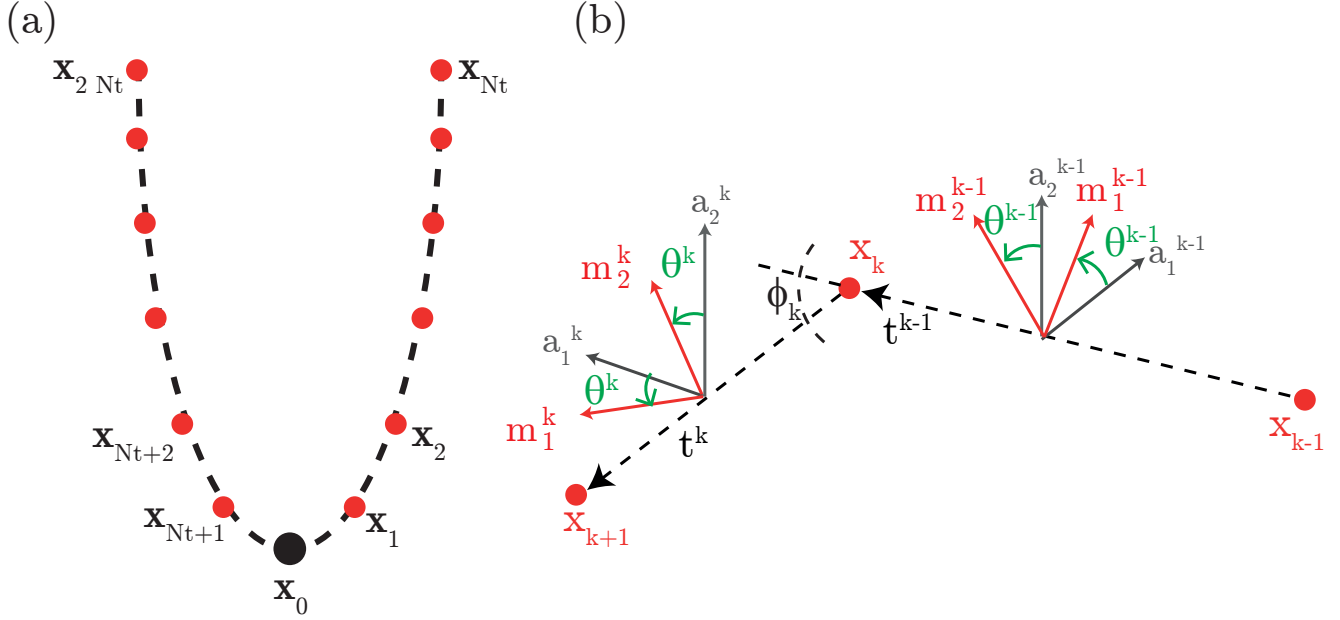


FIG. 2: (a) Discrete representation of a spider with 2 threads. (b) Three nodes, two edges, and the associated material and reference frames. Bending energy is related to the turning angle ϕ_k , twisting energy is related to $(\theta^k - \theta^{k-1})$, and stretching energy is related to the elongation of the edges.

104 In order to keep track of the rotation of the edges, the k -th edge in Figure 2(b) is decorated with an orthonormal
105 material frame, $(\mathbf{m}_1^k, \mathbf{m}_2^k, \mathbf{t}^k)$, where \mathbf{t}^k is the unit normal vector parallel to \mathbf{e}^k (i.e. tangent along the k -th edge).
106 Since this frame always has the third director parallel to the tangent, it is an “adapted” frame. A reference frame
107 $(\mathbf{a}_1^k, \mathbf{a}_2^k, \mathbf{t}^k)$ – another orthonormal adapted frame – is also associated with each edge. At time $t = 0$, the reference
108 frame and the material frame are identical. During the time marching scheme of the simulation (Algorithm 1), the
109 reference frame is updated through parallel transport in time. Parallel transport is the *most natural* or *twist free* way
110 of moving an adapted frame from one edge to another; details can be found in Refs. [25, 28]. Using the reference frame,
111 the material frame can be fully described using a single scalar quantity – the twist angle, θ^k , – which is the signed
112 angle from \mathbf{a}_1^k to \mathbf{m}_1^k about the tangent \mathbf{t}^k . As the reference frame is changing with time by time parallel transport,
113 twist may accumulate in the reference and this so-called reference twist has to be accounted for when calculating the
114 twist of the material frame.

115 The degrees of freedom (DOF) vector ξ of the spider with $n_t N_t + 1$ nodes and $n_t N_t$ edges has a size of $\text{ndof} =$
116 $3 \times (n_t N_t + 1) + n_t N_t$ and is defined as:

$$\xi = [\mathbf{x}_0, \mathbf{x}_1, \mathbf{x}_2, \dots, \mathbf{x}_{n_t N_t}, \theta^0, \theta^1, \dots, \theta^{n_t N_t - 1}]^T, \quad (6)$$

117 where the superscript T denotes transpose. The equation of motion at each DOF is

$$m_i \frac{\partial^2 \xi_i}{\partial t^2} + \frac{\partial E_{\text{elastic}}}{\partial \xi_i} - f_i^{\text{ext}} = 0, \quad (7)$$

118 where $i = 1, \dots, \text{ndof}$, E_{elastic} is the elastic energy responsible for the stretching and bending, f_i^{ext} is the external
 119 force (or moment for twist angles), e.g. gravity, and m_i is the lumped mass at each DOF. The lumped mass at
 120 the head node which represents the spider mass is m_s ; the mass on the other nodes is computed using the density
 121 of thread ρ_t , its cross-sectional radius r_t and the length of the discrete edges. For the DOFs representing rotation
 122 (twist angles), the lumped mass is $\frac{1}{2}\Delta m r_t^2$, where Δm is the mass of an edge and r_t is the silk thread radius. The
 123 simulation discretizes time into small steps and Δt is the time step size. The equation of motion to march from $t = t_j$
 124 to $t = t_{j+1} = t_j + \Delta t$ is

$$f_i \equiv \frac{m_i}{\Delta t} \left[\frac{\xi_i(t_{j+1}) - \xi_i(t_j)}{\Delta t} - \dot{\xi}_i(t_j) \right] + \frac{\partial E_{\text{elastic}}}{\partial \xi_i} - f_i^{\text{ext}} = 0, \quad (8)$$

125 where f_i is the force exerted on each node. The *old* DOF $\xi_i(t_j)$ and velocity $\dot{\xi}_i(t_j)$ from the previous time step are
 126 known, E_{elastic} is the elastic energy evaluated at $\xi_i(t_{j+1})$, and f_i^{ext} is the external force evaluated at $\xi_i(t_{j+1})$.

127 In the simulations reported in this paper, number of nodes per threads is $N_t = 10^2$ and the time step size, Δt , is
 128 always less than 10^{-1} s. We use an adaptive time stepping scheme where the time step size is automatically reduced
 129 by a factor of 10 if the simulation fails to converge and is increased by a factor of 10 (but always less than 10^{-1} s) if
 130 the simulation runs successfully for approximately 10 time steps.

131 The Jacobian for equation 8 is

$$\mathbb{J}_{ij} = \frac{\partial f_i}{\partial \xi_j} = \mathbb{J}_{ij}^{\text{inertia}} + \mathbb{J}_{ij}^{\text{elastic}} + \mathbb{J}_{ij}^{\text{ext}}, \quad (9)$$

132 where

$$\mathbb{J}_{ij}^{\text{inertia}} = \frac{m_i}{\Delta t^2} \delta_{ij}, \quad (10)$$

$$\mathbb{J}_{ij}^{\text{elastic}} = \frac{\partial^2 E_{\text{elastic}}}{\partial q_i \partial q_j}, \quad (11)$$

$$\mathbb{J}_{ij}^{\text{ext}} = -\frac{\partial f_i^{\text{ext}}}{\partial q_j}. \quad (12)$$

133 Here, δ_{ij} represents Kronecker delta. We can solve the ndof equations of motion in equation 8 to obtain the *new*
 134 DOF $\xi(t_{j+1})$. The new velocity is simply

$$\dot{\xi}(t_{j+1}) = \frac{\xi(t_{j+1}) - \xi(t_j)}{\Delta t}. \quad (13)$$

135 Evaluation of the gradient of the elastic energy ($\frac{\partial E_{\text{elastic}}}{\partial \xi_i}$) as well as its Hessian ($\frac{\partial^2 E_{\text{elastic}}}{\partial \xi_i \partial \xi_j}$) are well documented in
 136 Refs. [25, 28, 29]. Bending energy is associated with the *turning angle* (ϕ_k in Figure 2) at the *internal nodes* on each
 137 thread, e.g. in case of the j -th thread, the associated nodes are $\mathbf{x}_{(j-1)N_t+1}, \mathbf{x}_{(j-1)N_t+2}, \dots, \mathbf{x}_{jN_t-1}$. Twisting energy
 138 is associated with the same nodes. Stretching energy is associated with each edge.

139 Unique to the problem of ballooning of spiders is the external forces, described next. Four types of external forces
 140 are acting on the rod network such that the ndof -sized external force vector (cf. equation 8) is

$$\mathbf{f}^{\text{ext}} = \mathbf{W} + \mathbf{F}_v + \mathbf{F}_r + \mathbf{F}_l, \quad (14)$$

141 where the term \mathbf{W} is the weight vector which can be trivially computed from the weight of the spider body, the density
 142 of the threads, and their cross-sectional radius. The viscous force term \mathbf{F}_v exerted by the surrounding air on the k -th
 143 node (cf. Figure 2(b)) to march from $t = t_j$ to $t = t_{j+1} = t_j + \Delta t$. Following Gray and Hancock's RFT [30, 31], the
 144 force on the node is

$$\mathbf{F}_{v,k} = (-\eta_{\parallel} + \eta_{\perp}) \mathbf{t}_k \mathbf{t}_k^T \Delta l \mathbf{v}_k - \eta_{\perp} \Delta l \mathbf{v}_k, \quad (15)$$

145 where Δl is the Voronoi length ($\frac{l_t}{N_t}$ for the internal nodes on the thread and $\frac{l_t}{2N_t}$ for the terminal nodes), \mathbf{t}_k is the
 146 node-based tangent (average of the tangents on the edge before and the edge after the k -th node), $\mathbf{v}_k = \frac{\mathbf{x}_k(t_{j+1}) - \mathbf{x}_k(t_j)}{\Delta t}$
 147 is the velocity of the k -th node, and the Resistive Force coefficients are

$$\eta_{\parallel} = \frac{2\pi\mu}{\log\left(\frac{l_t}{r_t}\right) - \frac{1}{2}}, \quad (16)$$

$$\eta_{\perp} = \frac{4\pi\mu}{\log\left(\frac{l_t}{r_t}\right) + \frac{1}{2}}, \quad (17)$$

148 where μ is the dynamic viscosity of air.

149 Note that η_{\perp} is approximately twice of η_{\parallel} , i.e. the resistance from drag is lower when the motion is along the tangent
 150 and higher when the motion is perpendicular to the tangent. The force calculated at each node using equation 15
 151 used to populate the ndof-sized viscous force vector, \mathbf{F}_v .

152 The spider body is assumed spherical, and thus the drag force at x_0 is computed using Stokes law given as follows:

$$F_{v,0} = 6\pi\mu r_s v_s \quad (18)$$

153 where r_s is the sphere radius and v_s is the spider body speed.

154 It should be noted that RFT is a simplification that ignored the hydrodynamic interaction induced by distant parts
 155 of one or multiple threads. This is in contrast with more accurate slender body theories (SBT) [32] that capture this
 156 interaction. While recent works [33] have combined DER with SBT, RFT seems to be reasonably accurate when the
 157 rod has a low curvature [32]. Further, RFT can be included in the simulation using the backward Euler's method
 158 (i.e. the gradient of the external force with respect to the DOFs in equation (12) is known). This is not the case
 159 when SBT is used and the SBT-derived force has to be incorporated using the forward Euler's method. Moreover,
 160 SBT requires solving a dense linear system of size ndof; this worsens the time complexity of the algorithm. The
 161 interaction between the flows induced by the head and the threads has also been ignored in our setup. It is possible
 162 to incorporate this interaction [34] at the expense of computational efficiency. However, in this study, the aim is to
 163 explore the essential physics of the ballooning phenomenon by parameter space exploration in numerical simulations
 164 and therefore a computationally efficient framework with DER and RFT has been chosen. A more comprehensive
 165 model is an interesting direction for future research.

166 The term \mathbf{F}_r in equation (14) is the Coulomb repulsion force on the k -th node given as:

$$\mathbf{F}_{r,k} = k_e \sum_{i \neq 0, i \neq k} \frac{q_i q_k}{r_{i,k}^3} \mathbf{r}_{i,k}, \quad (19)$$

167 where $r_{i,k} = \|\mathbf{x}_i - \mathbf{x}_k\|$ is the Euclidean norm of the distance between two nodes, $k_e = 9 \times 10^9 \text{ Nm}^2\text{C}^{-2}$ is the Coulomb
 168 constant, and q_i is the charge located at the i -th node. At the first node (spider body), the charge is $q_0 = Q_s$, where
 169 Q_s is the spider body electric charge. For all the other nodes (nodes on the thread of the spider), q_i can be computed
 170 from the total thread charge Q_t . Two cases will be discussed in Section III B. In the first case, the electric charge is
 171 located at the thread tip and $q_i = Q_t$ at the tip nodes (\mathbf{x}_{Nt} and \mathbf{x}_{2Nt} in Fig. 2); $q_i = 0$ otherwise. In the second case,
 172 the electric charge is uniformly distributed along the thread and $q_i = Q_t \Delta l / l_t$, where Δl is the length of each edge
 173 and l_t is the length of each thread. The force calculated at each node using equation 19 then constitutes the Coulomb
 174 repulsion vector, \mathbf{F}_r , of size ndof.

175 Finally the electrostatic lift term \mathbf{F}_l which only acts along the z -axis. At the k -th node on the rod network, the lift
 176 force vector (size 3) is

$$\mathbf{F}_{l,k} = \begin{bmatrix} 0, \\ 0, \\ E_k q_k \end{bmatrix}, \quad (20)$$

177 where E_k is the electric potential evaluated at z -coordinate of the node, \mathbf{x}_k , at $t = t_{j+1}$ from equation (22), and
 178 q_k is the charge located at the k -th node. The charge located on the head node, \mathbf{x}_0 , is different than the charges
 179 located on the thread nodes. After calculating the forces on each node, the ndof-sized electrostatic lift force, \mathbf{F}_l , can
 180 be constructed.

181 In the force expressions above, we did not explicitly write down the Jacobian terms (e.g. derivative of the forces
 182 with respect to the DOFs). However, derivation of the Jacobian terms related to these external forces require is rather
 183 trivial.

184 The main steps of the algorithm are outlined below in Algorithm 1.

Algorithm 1 Discrete Elastic Rods

```

Require:  $\xi(t_j), \dot{\xi}(t_j)$  ▷ DOFs and velocities at  $t = t_j$ 
Require:  $(\mathbf{a}_1^k(t_j), \mathbf{a}_2^k(t_j), \mathbf{t}^k(t_j))$ ,  $k \in [0, n_t N_t - 1]$  ▷ Reference frame at  $t = t_j$ 
Ensure:  $\xi(t_{j+1}), \dot{\xi}(t_{j+1})$  ▷ DOFs and velocities at  $t = t_{j+1}$ 
Ensure:  $(\mathbf{a}_1^k(t_{j+1}), \mathbf{a}_2^k(t_{j+1}), \mathbf{t}^k(t_{j+1}))$ ,  $k \in [0, n_t N_t - 1]$  ▷ Reference frame at  $t = t_{j+1}$ 

1: function DISCRETE_ELASTIC_RODS(  $\xi, \dot{\xi}(t_j), (\mathbf{a}_1^k(t_j), \mathbf{a}_2^k(t_j), \mathbf{t}^k(t_j))$  )
2:   Guess:  $\xi^{(1)}(t_{j+1}) \leftarrow \xi(t_j)$ 
3:    $n \leftarrow 1$ 
4:   while error > tolerance do
5:     Compute reference frame  $(\mathbf{a}_1^k(t_{j+1}), \mathbf{a}_2^k(t_{j+1}), \mathbf{t}^k(t_{j+1}))^{(n)}$  using  $\xi^{(n)}(t_{j+1})$ 
6:     Compute reference twist  $\Delta m_{k,\text{ref}}^{(n)}$  at each internal node
7:     Compute material frame  $(\mathbf{m}_1^k(t_{j+1}), \mathbf{m}_2^k(t_{j+1}), \mathbf{t}^k(t_{j+1}))^{(n)}$ 
8:     Compute  $\mathbf{f}$  and  $\mathbb{J}$  ▷ Equations. 8 and 9
9:      $\Delta \xi \leftarrow \mathbb{J} \backslash \mathbf{f}$  ▷ Newton-Raphson method
10:     $\xi^{(n+1)} \leftarrow \xi^{(n)} - \Delta \xi$  ▷ Update DOFs
11:    error  $\leftarrow \text{sum}(\text{abs}(\mathbf{f}))$ 
12:     $n \leftarrow n + 1$ 
13:  end while

14:   $\xi(t_{j+1}) \leftarrow \xi^{(n)}(t_{j+1})$ 
15:   $\dot{\xi}(t_{j+1}) \leftarrow \frac{\xi(t_{j+1}) - \xi(t_j)}{\Delta t}$ 
16:   $(\mathbf{a}_1^k(t_{j+1}), \mathbf{a}_2^k(t_{j+1}), \mathbf{t}^k(t_{j+1})) \leftarrow (\mathbf{a}_1^k(t_{j+1}), \mathbf{a}_2^k(t_{j+1}), \mathbf{t}^k(t_{j+1}))^{(n)}$ 
17:  return  $\xi(t_{j+1}), \dot{\xi}(t_{j+1}), (\mathbf{a}_1^k(t_{j+1}), \mathbf{a}_2^k(t_{j+1}), \mathbf{t}^k(t_{j+1}))$ 
18: end function

```

185

C. Validation for Single Thread

186 In this section we validate the results computed numerically for a single thread case with those obtained by
 187 Gorham [19] and Morley and Gorham [22]. In their studies, a spider with a single thread was assumed, thus,
 188 the repelling forces between the threads are not considered in their models.

189 In the first validation study, the electric potential field given in equation (21) is adopted as in the theoretical analysis
 190 of Gorham [19]. Gorham [19] used an approximated analytical model for the atmospheric electric field as it varies
 191 with the altitude from flat earth surface on a normal day:

$$E = E_0 e^{-\alpha z} \quad (21)$$

192 where $E_0 = -120 \text{ Vm}^{-1}$ is the reference electric field at zero altitude, $\alpha = 3 \times 10^{-4} \text{ m}^{-1}$ and z is the altitude in m.

193 Simulations are carried out by spanning spiders with masses from 0.1 to 2 mg and thread electric charge from 10
 194 to 200 nC. We observe the vertical velocity of the spider; if this velocity is positive this means that ballooning will
 195 eventually take place. If the velocity is negative it means that the spider will be in a free fall. Figure 3 shows the
 196 contour of vertical velocity versus spider mass and electric charge in addition to the required thread charge to obtain
 197 ballooning found theoretically by Gorham [19] and which corresponds to 100 nC/mg of spider mass. From this figure,
 198 it is observed that the terminal ballooning velocity reaches up to 1.2 m/s for small spiders weighting 0.1 mg and
 199 having a thread charge of 200 nC. From the present numerical simulations the required ballooning for single thread
 200 spider is around 86 nC/mg which is 14 % different than that obtained by Gorham [19] theoretical analysis which was
 201 simplified by assuming a ballooning acceleration of 3 m/s^2 and neglected viscous effects.

202 Thus in the second validation we consider the experimental measurement coupled to 1-D numerical simulations
 203 of ballooning spiders performed by Morley and Gorham [22] inside a controlled closed chamber. In their study, the
 204 electric potential field is computed using a commercial electromagnetic simulation software. The resulting electric
 205 potential obtained in [22] is fitted here using the following exponential function and implemented in our simulations:

$$E = E_1 \exp(-z/z_1) + E_2 \exp(-z/z_2) + E_0, \quad (22)$$

206 where $E_0 = 7.41 \times 10^3 \text{ V/m}$, $E_1 = 2.52 \times 10^5 \text{ V/m}$ and $z_1 = 1.51 \times 10^{-3} \text{ m}$, $E_2 = 5.07 \times 10^4 \text{ V/m}$ and $z_2 = 7.93 \times 10^{-3} \text{ m}$.
 207 Following this linear regression model adopted in equation (22), the R^2 value is around 0.9973, which is evidence of
 208 the good fitting.

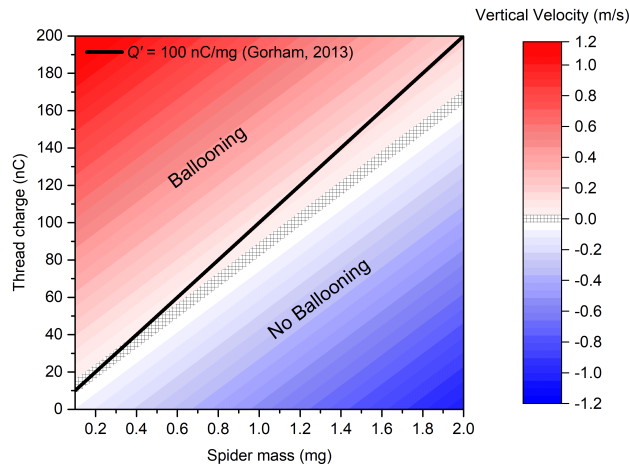


FIG. 3: Contour of vertical velocity versus spider mass and charge electric charge. The black solid line corresponds to the required charge for ballooning per 1 mg of spider mass obtained theoretically by Gorham [19]. The hatched region in the plot corresponds to the 86 nC/mg of required charge for ballooning obtained from present numerical simulations.

209 It is worthy to note that Morley and Gorham [22] used an aluminum-foil covered prominence in order to concentrate
 210 the electric field near the tip. The electric potential obtained from equation 22 is compared to that adopted by
 211 Morley and Gorham [22] in Figure 4. This figure shows a good agreement between the electric potential obtained
 212 from equation 22 with that used by Morley and Gorham [22]. The Earth's electrostatic field is on average much
 213 weaker than the one presented in equation 22; however, Morley and Gorham [22] pointed out the large variations in
 214 electrostatic field strength due to atmospheric activity that can generate the necessary lift for ballooning. The lift
 215 necessary for ballooning will be explored later in this paper (Figure 6).

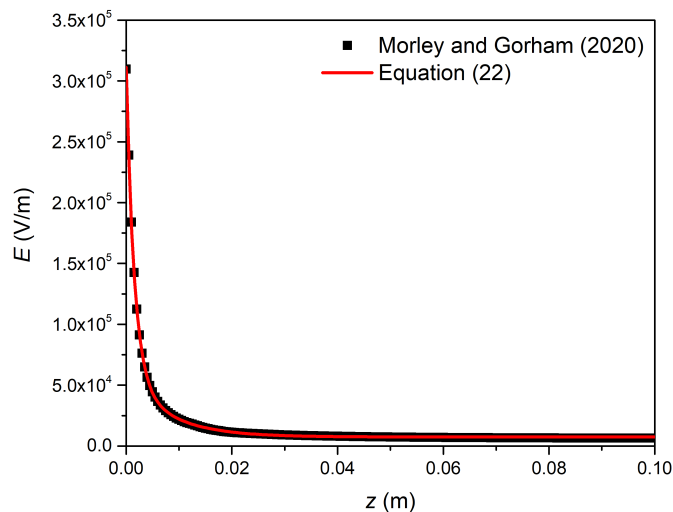


FIG. 4: Comparison of the electric potential obtained using equation. 22 and that adopted in Morley and Gorham [22]

216 According to Morley and Gorham [22], the total required ballooning charge is around 1.28 nC/mg which is much
 217 smaller than that obtained by Gorham [19] due to higher electric potential field at the tip of the prominence that
 218 builds the electric field. In this simulation we consider a single 1 thread of length 0.5 m as in [22].

219 Figure 5 shows the comparison of the actual computed results for the vertical spider ballooning distance and the
 220 vertical spider ballooning velocity with those obtained experimentally by Morley and Gorham [22]. In Figure 5 (a), it is
 221 observed that the ballooning distance obtained in the present study corresponds well to that obtained experimentally.

222 The comparison with the velocity in Figure 5 (b) shows a fair agreement between the present computed results and
 223 those obtained experimentally by Morley and Gorham [22]. It is observed that the spider is ejected promptly from
 224 the prominence where its velocity stabilizes at 8.5 cm/s after around 0.1 second.

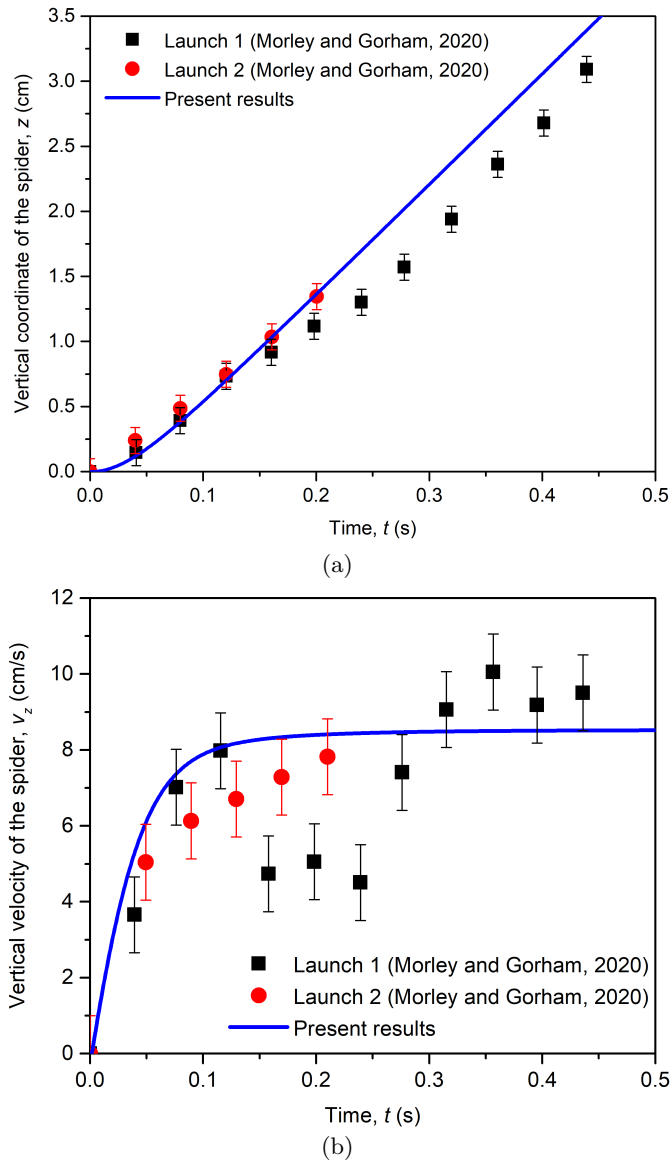


FIG. 5: (a) Vertical coordinate of the spider and (b) its vertical velocity compared to those obtained from Morley and Gorham [22]

225

III. RESULTS

226 In this section we present the results for ballooning velocity and thread unfolding dynamics. The electric field given
 227 in equation 22 is adopted.

228

A. Normalized Quantities

229 From principles of dimensional analysis, the ballooning phenomenon can be represented as a function of a number
 230 of non-dimensional (i.e. normalized) parameters. Hereon, we present our results in terms of normalized parameters.

231 First, we introduce the relevant normalized quantities.

- **Normalized terminal velocity.** Let us formulate a characteristic velocity, v_{charac} , from a scaling analysis based on the balance of forces along the z -axis. The force along the positive z -axis is $Q_t E_0 - W_s$, with $Q_t E_0$ the lift force and W_s the spider weight (weight of the threads is negligible) and the viscous force along the negative z scales as $\sim \mu n_t l_t v_{\text{charac}}$. Note that this viscous force is simply an estimate; the exact value depends on the deformed configuration of the threads and the Resistive Force coefficients. Balancing these forces, we get

$$Q_t E_0 - W_s = \mu n_t l_t v_{\text{charac}};$$

this leads to

$$v_{\text{charac}} = \frac{Q_t E_0 - W_s}{\mu l_t n_t}.$$

232 Since the above characteristic velocity is derived from a simple scaling analysis, the terminal velocity of the
233 spider, v_t , is expected to be on the same order of magnitude as (but not exactly equal to) v_{charac} . The terminal
234 velocity is normalized by this characteristic velocity to obtain the normalized terminal velocity,

$$\bar{v}_t = \frac{v_t}{v_{\text{charac}}} = \frac{\mu v_t n_t l_t}{Q_t E_0 - W_s}. \quad (23)$$

- **Normalized viscous force.** The viscous force scales as $F_v = \mu l_t^2 / t_{\text{charac}}$ and we use $t_{\text{charac}} = \sqrt{l_t/g}$ as the characteristic time. Physically, the time taken by a spider to fall a distance of l_t in a viscosity-free environment under the influence of gravity is the characteristic time, t_{charac} . This follows from the kinematic equation of free fall: $l_t \sim g t_{\text{charac}}^2$. An estimate of the magnitude of the Coulomb repulsion force is $F_r = k_e Q_t^2 / [n_t^2 l_t^2]$. This estimate is obtained from equation (19) under the assumption that two point charges of Q_t/n_t magnitude are located at a distance equal to the spider silk length, l_t . Normalizing the viscous force by the Coulomb repulsion force, we get the normalized viscous force,

$$\bar{F}_v = \frac{F_v}{F_r} = \frac{\mu n_t^2 \sqrt{g} l_t^{7/2}}{k_e Q_t^2} \quad (24)$$

- **Normalized lift force.** As sufficiently high altitude ($z \gg z_0$ in equation 22), the lift force scales as $Q_t E_0$. We normalize this by the weight of the spider to get the normalized lift force.

$$\bar{F}_l = \frac{Q_t E_0}{W_s} \quad (25)$$

244 Lift is equal to weight when $\bar{F}_l = 1$, assuming that the altitude is sufficiently high. If lift is larger than weight
245 so that $\bar{F}_l > 1$, the spider is expected to move up in altitude. On the other hand, if $\bar{F}_l < 1$, its altitude will
246 decrease.

- **Normalized bending stiffness.** The characteristic bending force YI/l_t^2 is normalized by the characteristic Coulomb repulsion force $F_r = k_e Q_t^2 / [n_t^2 l_t^2]$ to get the normalized bending stiffness,

$$\bar{YI} = \frac{n_t^2 YI}{k_e Q_t^2}. \quad (26)$$

249 If the normalized bending stiffness is very small compared with 1 ($\bar{YI} \ll 1$), the elastic stiffness of the threads
250 offers no resistance against deformation due to Coulomb repulsion force. The threads behave almost like a
251 viscous fluid in this case without any noticeable effect of elastic stiffness on the final shape. The other extreme
252 is $\bar{YI} \gg 1$ when the threads are too rigid to have any deformation under Coulomb repulsion force.

253 The normalized lift force is varied by varying the total threads electric charge between 0.5 and 5 nC. The number
254 of threads n_t considered in this study are 1, 2, 4 and 8. Biologically, the number of threads observed in ballooning
255 spiders range from 2 to 100 [17, 35, 36]. However, to be able to explore the main physics of the spiders ballooning by
256 parameter space exploration, and due to the associated computational limitations, the number of threads is limited
257 to 8. Moreover, it is found that beyond 8 threads, there is no significant effect on the normalized terminal ballooning
258 velocity of the spider as well as on the normalized lift and viscous forces.

B. Ballooning Velocity

259

260 In this section we present the variation of the normalized terminal ballooning velocity \bar{v}_t in terms of normalized lift
 261 force \bar{F}_l , normalized viscous force \bar{F}_v and normalized bending stiffness \bar{YI} for different number of threads and for two
 262 cases:

- 263 • Electric charge located at the thread tip, as suggested by Morley and Gorham [22]
- 264 • Electric charge is uniformly distributed along the threads

265 In Figure 6 we compare the variation of \bar{v}_t in terms of the normalized lift force for varying number of threads. This
 266 figure shows how the spider elicit ballooning once the normalized lift force exceeds 1. When the lift force is below 1,
 267 the ballooning velocity is zero since the spider cannot fly when the lift force generated by the electric potential field
 268 is smaller than the spider weight. For the tip located electric charge, the normalized terminal velocity slightly falls
 269 linearly with increasing normalized lift force. Referring to equation 23, this implies that the dimensional velocity v_t
 270 increases linearly with the dimensional lift force $Q_t E_0$. On the other hand, for the uniform distributed thread charge
 271 the normalized velocity shifts from that for the tip located charge and decreases when the normalized lift force exceeds
 272 1.5 with a slope around to $-1/3$, i.e. the dimensional velocity will increase with the dimensional lift force with a slope
 273 of approximately $2/3$ according to equation (23). This dependence is caused by an intricate interplay between the
 274 Coulomb repulsion force, electrostatic lift force and the viscous drag. The repulsion force causes the threads to spread
 275 far apart from one another, i.e. all the threads would assume a horizontal configuration if the repulsion force was the
 276 only force acting on them. However, the shape of the thread influences the amount of viscous drag. According to the
 277 RFT, drag is the lowest when velocity is parallel to the tangent on the thread (i.e. the threads are vertical) and it is
 278 the highest when velocity is perpendicular to the tangent (i.e. the threads are horizontal). These competing forces
 279 cause the threads to deform to eventually find a configuration where all the forces sum to zero. Our simulation tool
 280 essentially solves this balance of forces and updates the configuration of the threads over time.

281 It is observed in this figure that for the one thread case and for $\bar{F}_l > 1$, the normalized terminal velocity stabilizes
 282 at around 2.2 while for the other cases with higher number of threads, the normalized terminal velocity reaches values
 283 around 2 for the tip located charge, and values around 1.7 for the uniformly distributed charge, especially for higher
 284 \bar{F}_l . This further highlights the role of the deformed shape of the threads in common spider ballooning process. When
 285 there is only one thread, it is oriented vertically and thus experiences the least amount of drag. When multiple threads
 286 are introduced, the threads deform due to the Coulomb repulsion force and the threads are no longer oriented parallel
 287 to the direction of velocity. As such, more drag is exerted by air on the threads and the velocity is reduced in the
 288 case of still air. Meanwhile, the 3D conical thread net shape would lead to an increase in the ballooning speed in case
 289 of updraft wind caused by natural convection for instance.

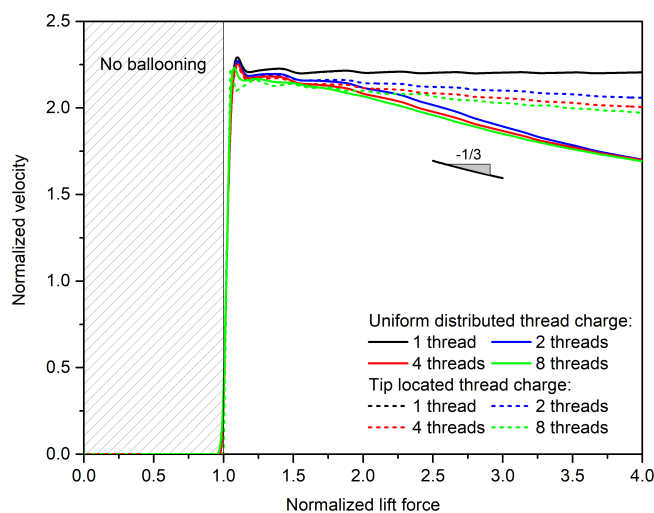


FIG. 6: Variation of the normalized terminal ballooning velocity versus normalized lift for a given value of normalized bending stiffness

290 In the present study we considered *Erigon* spiders which are relatively small where their mass is about 1 mg and
 291 a size around 1 cm. Meanwhile, Schneider *et al.* [36], observed the ballooning of *Stegodyphus dumicola* (Eresidae)

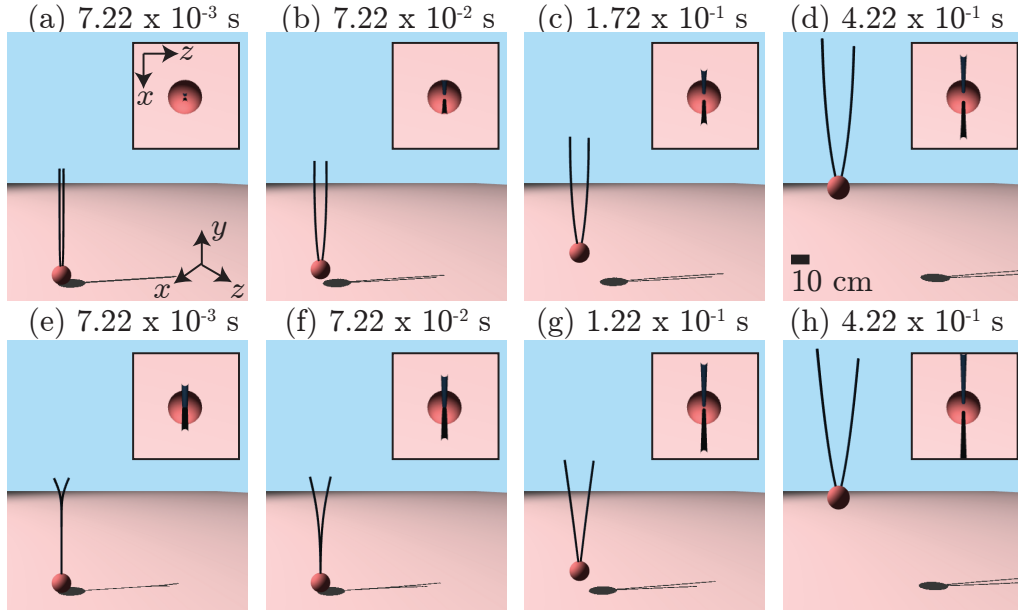


FIG. 7: Unfolding dynamics of two spider threads with uniformly distributed (a-d) and tip located (e-h) electric charge. Insets show the top view ($x - z$ plane) of the threads.

292 Pocock spiders weighting 100 mg and of size 7 to 14 mm. These spiders were found to balloon using 100 threads
 293 forming a triangular sheet with a length and width of about 1 m at the distal end. In the present study, we limited
 294 the number of silk threads to 8 due to computational limitations. However, referring to Figure 6, we can see that the
 295 normalized terminal velocity becomes somehow independent from the number of threads when they exceed 8. And
 296 thanks to the normalized analysis, we can generalize our study to verify Schneider *et al.* [36] observation regrading
 297 the ballooning of large spiders.

298 Using Figure 6 and data from Schneider *et al.* [36], we can deduce that if the spiders were on flat earth ground,
 299 where the electric field is 100 V/m, the electrostatic charge required for ballooning is around 100 nC per thread. From
 300 our simulations, it is observed that this very large electrostatic charge on the silk thread will lead to high Coulomb
 301 repelling forces which will cause the threads to repel diametrically in a plane which is in contradiction to Schneider *et*
 302 *al.* [36] observations. Meanwhile, assuming the spiders are hanging on the top of tree branches where the electric field
 303 can reach 100 kV/m, the spider needs 0.1 nC per thread to balloon. It is worthy to note that Schneider *et al.* [36]
 304 studies were done in farm Omdraai, Namibia which has very few trees. Moreover, the air temperature was reaching
 305 33.8° with almost no wind, a situation in favor for rising thermal currents. Thus, based on our conclusion and on
 306 Schneider *et al.* [36] observations, for large spiders to balloon, rising thermal currents seem to be essential. In our
 307 study, we do not eliminate the fact that wind, turbulence and thermal currents could cause ballooning, however, we
 308 shed light on that these electrostatic forces could be alone used to balloon small spiders and that they are responsible
 309 on repelling the threads to avoid entanglement.

310 Referring to equation (23), and assuming that the following parameters are unchanged during typical ballooning:
 311 thread electric charge, Q_t , the atmospheric electric field, E_0 , the air viscosity, μ and the spider weight, W_s , the spider
 312 could control its ballooning velocity by varying the thread length, l_t and the number of threads. In the presence of
 313 significant wind speed, the spider could also control the flight altitude and direction by varying the number and length
 314 of ballooning threads. For instance, longer threads can result in larger drag forces and thus higher altitude in case of
 315 updraft wind. Reducing the length and number of threads could then be used during landing process.

316 The variation of the normalized terminal ballooning velocity, \bar{v}_t , versus normalized viscous force, \bar{F}_v for $Q_t = 2.5$ nC
 317 and $Y = 20 \times 10^9$ Pa was also analyzed. The viscous force was varied by varying the viscosity between 10^{-7} and
 318 10^{-3} Pa-s. It is observed that the normalized terminal ballooning velocity is always equal approximately to 2.12.
 319 This indicates that the normalized viscous forces do not play a major role in the ballooning of spiders once it reaches
 320 steady-state.

321 The variation of the normalized ballooning velocity, \bar{v}_t , versus normalized bending stiffness, \bar{YI} for $Q_t = 2.5$ nC and
 322 $\mu = 18.37 \times 10^{-6}$ Pa.s shows also that the normalized terminal ballooning velocity is always equal to approximately
 323 2.12. The normalized bending stiffness was varied by varying the Young's modulus of elasticity Y between 5 and
 324 50 GPa where the average known silk modulus of elasticity is around 25 GPa [37]. This indicates that the bending

325 stiffness, representative of the elasticity of the thread, does not play a major role in the ballooning of spiders. This
 326 is also anticipated from the ratio of characteristic bending force to characteristic Coulomb repulsion force. This ratio
 327 is defined as the normalized bending stiffness in equation 26 and its value in the regime relevant to ballooning is
 328 the order of 10^{-9} to 10^{-8} and, therefore, it is expected that the bending stiffness of the threads offers little resistance
 329 against deformation due to Coulomb repulsion force. We also observed in our simulations that the twisting and
 330 stretching deformation is negligible compared with bending mode. In summary, once the spider reaches a steady
 331 velocity after the transient dynamics, the velocity and the shape of the threads do not depend on the elastic bending,
 332 stretching, and twisting stiffness.

333 C. Thread unfolding Dynamics

334 The spider threads unfolding dynamics is shown in Figure 7 for the 2 threads case for better visibility. For the
 335 uniformly distributed thread charge it can be observed that the bending occurs along the threads which move apart
 336 gradually with an increase in their curvature until they reach a steady-state position with a v-shape as observed in
 337 real ballooning spiders.

338 For the case with tip located charge, the repelling force acts on the tips of the threads pushing them apart while
 339 maintained in close contact in the bottom region. After a short time, the threads make a v-shape similar to that
 340 of the previous case. The results are also accompanied with animations showing the time evolution of the unfolding
 341 dynamics (see Supplementary Material [38]).

342 Figure 8 shows the ballooning process and spider threads bending for two, four and eight threads. The threads
 343 are pushed apart due to the Coulomb electrostatic forces while the spider is moving upward due to the atmospheric
 344 electric field. A supplemental material also shows an animation of the multi-threaded spider ballooning and unfolding
 345 dynamics [38].

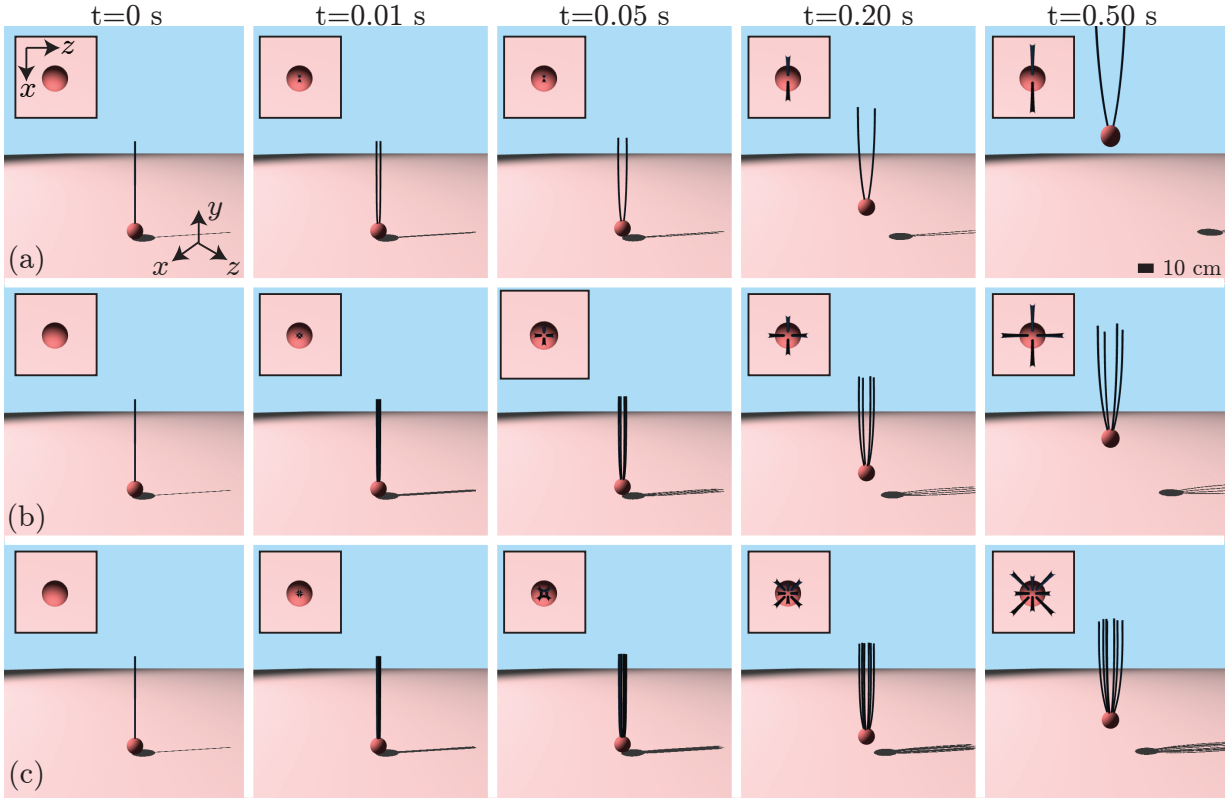


FIG. 8: Ballooning process obtained from our 3D numerical simulations for spider with (a) two threads, (b) four threads and (c) eight threads. Insets show the top view ($x - z$ plane) of the threads. A supplemental animation is also attached to the paper [38] ([click here to play video](#))

IV. CONCLUSION

347 Three dimensional numerical simulations are performed for spider ballooning due to electrostatic forces. Spiders with
 348 multi silk threads are considered in this study. The numerical method of the fluid-structure-electric field interaction
 349 combines the DER algorithm to compute the elastic deformation of the spider threads. Moreover, the RFT is used
 350 to compute the hydrodynamic viscous forces on the spider and on the threads. The electrostatic forces caused by the
 351 atmospheric potential gradient and the thread electric charge is computed based on the Coulomb theory. The spider
 352 is approximated by a sphere attached to one or multiple silk threads. The numerical results computed in this paper
 353 are first validated against theoretical and experimental data from the open literature for one-thread case showing a
 354 good agreement.

355 Two cases were studied in this paper. In the first one, we assume that the thread charge is uniformly distributed
 356 along the threads. In the second, we assume that the charge is located at the thread tip.

357 The results show that for one thread case, the normalized velocity is around 2.2 and independent of the normalized
 358 lift and normalized viscous forces while it is slightly less for the multi-thread cases. In the uniformly distributed
 359 charge case, the normalized ballooning velocity deviates from that for the tip located charge and decreases slightly
 360 when the normalized lift force exceeds 2 with a slope equal to $-1/3$.

361 Finally, the Coulomb repelling forces cause the threads to bend and form a three-dimensional conical sheet very
 362 similar to observations from open literature. This bending behavior is very fast and occurs in the beginning of the
 363 ballooning process before it stabilizes at a steady-state shape.

364 It should be noted that the wind speed and its fluctuations could affect the behavior of trichobothria. In fact, the
 365 spiders use the deformation of trichobothria signal to determine whether they will balloon or not. Hence, for high
 366 wind speeds and fluctuations the signals of electric field could be buried and the spider may not be able to distinguish
 367 whether the deformation of trichobothria is caused by wind or by electric field. Therefore, spiders usually balloon on
 368 relatively calm days as explained earlier in the introduction section.

369 Moreover, in this study, the aim is to explore the essential physics of the spiders ballooning by parameter space
 370 exploration and therefore a computationally efficient framework with DER and RFT has been chosen. A more
 371 comprehensive model coupling for instance SBT and DER is an interesting direction for future research.

ACKNOWLEDGMENTS

372
 373 The authors would like to thank E.L. Morley from the University of Bristol and P.W. Gorham from the University
 374 of Hawaii at Manoa for providing the electric field data in the chamber where the experiments were done in reference
 375 [22] and used in the present paper to generate the electrostatic field model given in equation 22. M.K.J. acknowledges
 376 support from the National Science Foundation (Award numbers: CAREER-2047663, CMMI-2053971, CMMI-2101751,
 377 IIS-1925360).

-
- 378 [1] J. R. Bell, D. A. Bohan, E. M. Shaw, and G. S. Weyman, Ballooning dispersal using silk: world fauna, phylogenies, genetics
379 and models, *Bulletin of Entomological Research* **95**, 69 (2005).
- 380 [2] C. Darwin, *Journal of researches into the natural history and geology of the countries visited during the voyage of H.M.S.*
381 *Beagle round the world, under the Command of Capt. Fitz Roy*, 2nd ed. (J. Murray, 1845).
- 382 [3] M. Lister, Some observations concerning the odd turn of some shell snails and the darting of spiders, *Philosophical*
383 *Transactions of the Royal Society of London* **4**, 1011 (1669).
- 384 [4] J. Blackwall, Xx. observations and experiments, made with a view to ascertain the means by which the spiders that produce
385 gossamer effect their aerial excursions, *Transactions of the Linnean Society of London* **os-15**, 449 (1827).
- 386 [5] C. Richter, Aerial dispersal in relation to habitat in eight wolf-spider species (pardosa, araneae, lycosidae), *Oecologia* **5**,
387 200–214 (1970).
- 388 [6] J. T. Salmon and N. V. Horner, Aerial dispersion of spiders in north central texas, *The Journal of Arachnology* **5**, 153
389 (1977).
- 390 [7] G. S. Weyman, K. D. Sunderland, and P. C. Jepson, A review of the evolution and mechanisms of ballooning by spiders
391 inhabiting arable farmland, *Ethology Ecology & Evolution* **14**, 307 (2002).
- 392 [8] C. Darwin, *Charles Darwin's zoology notes and specimen lists from H. M. S. Beagle*, edited by R. Keynes (Cambridge
393 University Press, 2005).
- 394 [9] V. M. J. Lee, M. Kuntner, and D. Li, Ballooning behavior in the golden orbweb spider *nephila pilipes* (araneae: Nephilidae),
395 *Frontiers in Ecology and Evolution* **3**, 2 (2015).
- 396 [10] J. A. C. Humphrey, Fluid mechanic constraints on spider ballooning, *Oecologia* **73**, 469 (1987).
- 397 [11] R. Suter, Ballooning in spiders: results of wind tunnel experiments, *Ethology Ecology & Evolution* **3**, 13 (1991).
- 398 [12] R. Courtney, T. Stevens, W. Zhang, and L. Zhao, Flying spiders: What is the drag acting on a spider-dragline in free-fall?
399 (American Institute of Aeronautics and Astronautics, 2020).
- 400 [13] M. Cho, Aerodynamics and the role of the earth's electric field in the spiders' ballooning flight, *Journal of Comparative*
401 *Physiology A* **207**, 219–236 (2021).
- 402 [14] L. Zhao, I. Panayotova, A. Chuang, K. Sheldon, L. Bourouiba, and L. Miller, Flying spiders: simulating and modeling the
403 dynamics of ballooning, in *Women in Mathematical Biology*, edited by A. T. Layton and L. A. Miller (Springer International
404 Publishing, Cham, 2017) pp. 179–210.
- 405 [15] R. Suter, An aerial lottery: the physics of ballooning in a chaotic atmosphere, *The Journal of Arachnology* **27**, 281 (1999).
- 406 [16] A. Reynolds, D. Bohan, and J. Bell, Ballooning dispersal in arthropod taxa with convergent behaviours: dynamic properties
407 of ballooning silk in turbulent flows, *Biology letters* **2**, 371–373 (2006).
- 408 [17] M. Cho, P. Neubauer, C. Fahrenson, and I. Rechenberg, An observational study of ballooning in large spiders: Nanoscale
409 multifibers enable large spiders' soaring flight, *PLOS Biology* **16**, 1 (2018).
- 410 [18] K. Kronenberger and F. Vollrath, Spiders spinning electrically charged nano-fibres, *Biology Letters* **11**, 20140813 (2015).
- 411 [19] P. Gorham, Ballooning spiders: the case for electrostatic flight (2013) arXiv:1309.4731v2.
- 412 [20] K. Sheldon, L. Zhao, A. Chuang, I. N. Panayotova, L. Miller, and L. Bourouiba, Revisiting the physics of spider ballooning,
413 in *Women in Mathematical Biology*, edited by A. T. Layton and L. A. Miller (Springer International Publishing, Cham,
414 2017) pp. 163–178.
- 415 [21] E. Morley and D. Robert, Electric fields elicit ballooning in spiders, *Current Biology* **28**, 2324–2330 (2018).
- 416 [22] E. L. Morley and P. W. Gorham, Evidence for nanocoulomb charges on spider ballooning silk, *Phys. Rev. E* **102**, 012403
417 (2020).
- 418 [23] M. Cho, K. Affeld, P. Neubauer, and I. Rechenberg, Spiders' ballooning flight as a model for the exploration of hazardous
419 atmospheric weather conditions, in *Biomimetic and Biohybrid Systems - 7th International Conference, Living Machines*
420 *2018, Paris, France, July 17-20, 2018, Proceedings*, Lecture Notes in Computer Science, Vol. 10928, edited by V. Vouloutsi,
421 J. Halloy, A. Mura, M. Mangan, N. Lepora, T. Prescott, and P. Verschure (Springer, 2018) pp. 110–114.
- 422 [24] S. Stauffer, S. Coguill, and R. Lewis, Comparison of physical properties of three silks from *nephila clavipes* and araneus
423 *gemmoides*, *The Journal of Arachnology* **22**, 5 (1994).
- 424 [25] M. Bergou, B. Audoly, E. Vouga, M. Wardetzky, and E. Grinspun, Discrete viscous threads, in *ACM SIGGRAPH 2010*
425 *Papers*, SIGGRAPH '10 (Association for Computing Machinery, New York, NY, USA, 2010).
- 426 [26] J. Lighthill, Flagellar hydrodynamics, *SIAM Rev.* **18**, 161 (1976).
- 427 [27] M. Bergou, M. Wardetzky, S. Robinson, B. Audoly, and E. Grinspun, Discrete elastic rods, in *ACM SIGGRAPH 2008*
428 *Papers*, SIGGRAPH '08 (Association for Computing Machinery, New York, NY, USA, 2008).
- 429 [28] M. K. Jawed, A. Novelia, and O. O'Reilly, *A primer on the kinematics of discrete elastic rods* (Springer, 2018).
- 430 [29] J. Panetta, M. Konaković-Luković, F. Isvoranu, E. Bouleau, and M. Pauly, X-shells: A new class of deployable beam
431 structures, *ACM Transactions on Graphics (TOG)* **38**, 1 (2019).
- 432 [30] N. Coq, O. Du Roure, J. Marthelot, D. Bartolo, and M. Fermigier, Rotational dynamics of a soft filament: Wrapping
433 transition and propulsive forces, *Physics of Fluids* **20**, 051703 (2008).
- 434 [31] J. Gray and G. Hancock, The propulsion of sea-urchin spermatozoa, *Journal of Experimental Biology* **32**, 802 (1955).
- 435 [32] B. Rodenborn, C. Chen, H. Swinney, B. Liu, and H. Zhang, Propulsion of microorganisms by a helical flagellum, *Proceedings*
436 *of the National Academy of Sciences* **110**, E338 (2013).
- 437 [33] W. Huang and M. K. Jawed, Numerical simulation of bundling of helical elastic rods in a viscous fluid, *Computers and*
438 *Fluids* -, (2021).

- 439 [34] A. Thawani and M. S. Tirumkudulu, Trajectory of a model bacterium, *Journal of Fluid Mechanics* **835**, 252 (2018).
- 440 [35] W. Wickler and U. Seibt, Aerial dispersal by ballooning in adult *Stegodyphus mimosarum*, *Naturwissenschaften* **73**, 628
441 (1986).
- 442 [36] J. Schneider, J. Roos, Y. Lubin, and J. Henschel, Dispersal of *Stegodyphus dumicola* (Araneae, Eresidae): they do balloon after all!, *The Journal of Arachnology* **29**, 114 (2001).
- 443 [37] S. Hudson, V. Zhurov, V. Grbić, M. Grbić, and J. Hutter, Measurement of the elastic modulus of spider mite silk fibers
444 using atomic force microscopy, *Journal of Applied Physics* **113**, 154307 (2013).
- 445 [38] See supplemental material at [url will be inserted by publisher] for an animation of the multi-threaded spider ballooning
446 and unfolding dynamics, [url will be inserted by publisher].
447